

# A study of the radiative $K_L \rightarrow \pi^\pm e^\mp \nu \gamma$ decay and search for direct photon emission with the KLOE detector

The KLOE Collaboration

F. Ambrosino<sup>5,6</sup>, A. Antonelli<sup>1</sup>, M. Antonelli<sup>1</sup>, F. Archilli<sup>10,11</sup>, C. Bacci<sup>12,13</sup>, P. Beltrame<sup>2</sup>, G. Bencivenni<sup>1</sup>, S. Bertolucci<sup>1</sup>, C. Bini<sup>8,9</sup>, C. Bloise<sup>1</sup>, S. Bocchetta<sup>12,13</sup>, F. Bossi<sup>1</sup>, P. Branchini<sup>13</sup>, R. Caloi<sup>8,9</sup>, P. Campana<sup>1</sup>, G. Capon<sup>1</sup>, T. Capussela<sup>1</sup>, F. Ceradini<sup>12,13</sup>, F. Cesario<sup>12,13</sup>, S. Chi<sup>1</sup>, G. Chiefari<sup>5,6</sup>, P. Ciambione<sup>1</sup>, F. Crucianelli<sup>8</sup>, E. De Lucia<sup>1</sup>, A. De Santis<sup>8,9</sup>, P. De Simone<sup>1</sup>, G. De Zorzi<sup>8,9</sup>, A. Denig<sup>2</sup>, A. Di Domenico<sup>8,9</sup>, C. Di Donato<sup>6</sup>, B. Di Micco<sup>12,13</sup>, A. Doria<sup>6</sup>, M. Dreucci<sup>1,a</sup>, G. Felici<sup>1</sup>, A. Ferrari<sup>1</sup>, M.L. Ferrer<sup>1</sup>, S. Fiore<sup>8,9</sup>, C. Forti<sup>1</sup>, P. Franzini<sup>8,9</sup>, C. Gatti<sup>1</sup>, P. Gauzzi<sup>8,9</sup>, S. Giovannella<sup>1</sup>, E. Gorini<sup>3,4</sup>, E. Graziani<sup>13</sup>, W. Kluge<sup>2</sup>, V. Kulikov<sup>16</sup>, F. Lacava<sup>8,9</sup>, G. Lanfranchi<sup>1</sup>, J. Lee-Franzini<sup>1,14</sup>, D. Leone<sup>2</sup>, M. Martini<sup>1,7</sup>, P. Massarotti<sup>5,6</sup>, W. Mei<sup>1</sup>, S. Meola<sup>5,6</sup>, S. Miscetti<sup>1</sup>, M. Moulson<sup>1</sup>, S. Müller<sup>1</sup>, F. Murtas<sup>1</sup>, M. Napolitano<sup>5,6</sup>, F. Nguyen<sup>12,13</sup>, M. Palutan<sup>1</sup>, E. Pasqualucci<sup>9</sup>, A. Passeri<sup>13</sup>, V. Patera<sup>1,7</sup>, F. Perfetto<sup>5,6</sup>, M. Primavera<sup>4</sup>, P. Santangelo<sup>1</sup>, G. Saracino<sup>5,6</sup>, B. Sciascia<sup>1</sup>, A. Sciubba<sup>1,7</sup>, A. Sibidanov<sup>1</sup>, T. Spadaro<sup>1</sup>, M. Testa<sup>8,9</sup>, L. Tortora<sup>13</sup>, P. Valente<sup>9</sup>, G. Venanzoni<sup>1</sup>, R. Versaci<sup>1,7</sup>, G. Xu<sup>1,15</sup>

<sup>1</sup> Laboratori Nazionali di Frascati dell'INFN, Via E. Fermi, 40 – 00044 Frascati (Roma), Italy

<sup>2</sup> Institut für Experimentelle Kernphysik, Universität Karlsruhe, Germany

<sup>3</sup> Dipartimento di Fisica dell'Università, Lecce, Italy

<sup>4</sup> INFN Sezione di Lecce, Lecce, Italy

<sup>5</sup> Dipartimento di Scienze Fisiche dell'Università “Federico II”, Napoli, Italy

<sup>6</sup> INFN Sezione di Napoli, Napoli, Italy

<sup>7</sup> Dipartimento di Energetica dell'Università “La Sapienza”, Roma, Italy

<sup>8</sup> Dipartimento di Fisica dell'Università “La Sapienza”, Roma, Italy

<sup>9</sup> INFN Sezione di Roma, Roma, Italy

<sup>10</sup> Dipartimento di Fisica dell'Università “Tor Vergata”, Roma, Italy

<sup>11</sup> INFN Sezione di Roma Tor Vergata, Roma, Italy

<sup>12</sup> Dipartimento di Fisica dell'Università “Roma Tre”, Roma, Italy

<sup>13</sup> INFN Sezione di Roma Tre, Roma, Italy

<sup>14</sup> Physics Department, State University of New York, Stony Brook, USA

<sup>15</sup> Institute of High Energy Physics of Academica Sinica, Beijing, China

<sup>16</sup> Institute for Theoretical and Experimental Physics, Moscow, Russia

Received: 9 April 2008 / Revised version: 7 May 2008 /

Published online: 29 May 2008 – © Springer-Verlag / Società Italiana di Fisica 2008

**Abstract.** We present a measurement of the ratio  $R = \Gamma(K_{e3}^0; E_\gamma^* > 30 \text{ MeV}, \theta_\gamma^* > 20^\circ) / \Gamma(K_{e3}^0)$  and a first measurement of the direct emission contribution in semileptonic  $K_L$  decays. The measurement was performed at the DAΦNE  $\phi$  factory by selecting  $\phi \rightarrow K_L K_S$  decays with the KLOE detector. We use  $328 \text{ pb}^{-1}$  of data, corresponding to about 3.5 million  $K_{e3}^0$  events and about 9000  $K_{e3\gamma}^0$  radiative events. Our result is  $R = (924 \pm 23_{\text{stat}} \pm 16_{\text{syst}}) \times 10^{-5}$  for the branching ratio and  $\langle X \rangle = -2.3 \pm 1.3_{\text{stat}} \pm 1.4_{\text{syst}}$  for the effective strength parameter describing direct emission.

**PACS.** 13.20.Eb

## 1 Introduction

The study of radiative  $K_L$  decays provides information about the structure of the kaon and the opportunity to quantitatively test theories describing hadron interactions and decays, such as chiral perturbation theory ( $\chi$ PT). In

addition, the correct understanding of radiation in  $K_L$  decays is necessary for precision measurements of the fully-inclusive decay rates. These, in turn, are needed for studies of the decay dynamics and the determination of the CKM matrix element  $|V_{us}|$ .

Two different processes contribute to photon emission in kaon decays: inner bremsstrahlung (IB) and direct emission (DE). DE is radiation from intermediate hadronic

<sup>a</sup> e-mail: Marco.Dreucci@lnf.infn.it

states and is sensitive to hadron structure. The relevant kinematic variables for the study of radiation in  $K_{\ell 3}$  decays are  $E_\gamma^*$ , the energy of the radiated photon, and  $\theta_\gamma^*$ , its angle with respect to the lepton momentum in the kaon rest frame. The IB amplitudes diverge for  $E_\gamma^* \rightarrow 0$ . For  $K_{e3}$ , for which  $m_e \approx 0$ , the IB spectrum in  $\theta_\gamma^*$  is peaked near zero as well. The IB and DE amplitudes interfere. The contribution to the width from IB-DE interference is 1% or less of the purely IB contribution; the purely DE contribution is negligible. To disentangle the two components, we measure the double differential rate  $d^2\Gamma/dE_\gamma^* d\theta_\gamma^*$ .

In the  $\chi$ PT treatment of [1], DE is characterized by eight amplitudes,  $\{V_i, A_i\}$ , which in the one-loop approximation are real functions. These terms have similar photon energy spectra, with maxima around  $E_\gamma^* = 100$  MeV. This suggests a decomposition of the photon spectrum at  $\mathcal{O}(p^6)$  as in [1]:

$$\begin{aligned} \frac{d\Gamma}{dE_\gamma^*} &= \frac{d\Gamma_{\text{IB}}}{dE_\gamma^*} + \sum_{i=1}^4 \left( \langle V_i \rangle \frac{d\Gamma_{V_i}}{dE_\gamma^*} + \langle A_i \rangle \frac{d\Gamma_{A_i}}{dE_\gamma^*} \right) \\ &\simeq \frac{d\Gamma_{\text{IB}}}{dE_\gamma^*} + \langle X \rangle f(E_\gamma^*). \end{aligned} \quad (1)$$

The DE contributions are summarized in the function  $f(E_\gamma^*)$ , which represents the deviation from the IB spectrum. The parameter  $\langle X \rangle$  measures the effective strength of the DE.  $\mathcal{O}(p^6)$   $\chi$ PT calculations give  $\langle X \rangle = -1.2 \pm 0.4$ , a  $3\sigma$  indication that the IB-DE interference is destructive.<sup>1</sup> The low-energy constants (LECs) for the  $\mathcal{O}(p^6)$  terms are unknown. An educated guess of their size leads to the assignment of an uncertainty on  $\langle X \rangle$  of 30% of the  $\mathcal{O}(p^4)$  result [1].

A first attempt to measure the DE contribution was performed by the KTeV collaboration [3] using the model described in [4, 5] within the so-called soft-kaon approximation. However, as shown in [1], in this approximation there is insufficient sensitivity for the evaluation of the contribution from DE. In contrast, our fit to the double differential spectrum  $d^2\Gamma/dE_\gamma^* d\theta_\gamma^*$  allows us to isolate DE from IB.

We also measure the ratio  $R$ , conventionally defined as

$$R \equiv \frac{\Gamma(K_{e3}^0; E_\gamma^* > 30 \text{ MeV}, \theta_\gamma^* > 20^\circ)}{\Gamma(K_{e3}^0)}, \quad (2)$$

where  $\Gamma(K_{e3}^0)$  represents the decay width inclusive of radiative effects. The value of this ratio has been computed at  $\mathcal{O}(p^6)$  in  $\chi$ PT, leading to the prediction [2]

$$R = (0.963 + 0.006\langle X \rangle \pm 0.010) \times 10^{-2}. \quad (3)$$

For  $\langle X \rangle = -1.2$ ,  $R = (0.96 \pm 0.01) \times 10^{-2}$ , as quoted in [1]. The simultaneous measurement of  $R$  and  $\langle X \rangle$  allows a precise comparison with the theory, in large part avoiding complications from the uncertainties on the LECs for  $\mathcal{O}(p^6)$ .

<sup>1</sup> The quantity  $\langle X \rangle$  was evaluated for  $\theta_\gamma^* > 5^\circ$  in [1], instead of  $\theta_\gamma^* > 20^\circ$  as in the present analysis. It turns out [2] that this makes a negligible difference.

In 2001, KTeV published [3] the result  $R = (0.908 \pm 0.008_{-0.012}^{+0.013}) \times 10^{-2}$ ; the data were subsequently reanalyzed using more restrictive cuts that provide better control over systematic effects, but which reduce the statistics by a factor of three. The more recent KTeV result [6] is  $R = (0.916 \pm 0.017) \times 10^{-2}$ . In 2005, NA48 [7] measured  $R = (0.964 \pm 0.008_{-0.009}^{+0.011}) \times 10^{-2}$ . Neither of these experiments measure  $\langle X \rangle$ .

## 2 Experimental setup

The data were collected with the KLOE detector at DAΦNE, the Frascati  $\phi$  factory. DAΦNE is an  $e^+e^-$  collider that operates at a center of mass energy of  $\sim 1020$  MeV, the mass of the  $\phi$  meson. Positron and electron beams of equal energy collide at an angle of  $(\pi - 0.025)$  rad, producing  $\phi$  mesons with a small momentum in the horizontal plane ( $p_\phi \sim 13$  MeV).  $\phi$  mesons decay  $\sim 34\%$  of the time into nearly collinear  $K_S K_L$  pairs; the detection of a  $K_S$  (the tagging kaon) therefore signals the presence of a  $K_L$  (the tagged kaon), independently of the decay mode of the latter. This principle is called  $K_L$  tagging in the following.

The KLOE detector consists of a large cylindrical drift chamber surrounded by a lead/scintillating-fiber electromagnetic calorimeter. A superconducting coil around the calorimeter provides a 0.52 T field. The drift chamber [8] is 4 m in diameter and 3.3 m long. The momentum resolution for tracks at large polar angles is  $\sigma_{p_\perp}/p_\perp \approx 0.4\%$ . The vertex between two intersecting tracks is reconstructed with a spatial resolution of  $\sim 3$  mm. The calorimeter [9] is divided into a barrel and two endcaps. It is segmented in depth into five layers and covers 98% of the solid angle. Energy deposits nearby in time and space are grouped into calorimeter clusters. The energy and time resolutions are  $\sigma_E/E = 5.7\%/\sqrt{E [\text{GeV}]}$  and  $\sigma_T = 57 \text{ ps}/\sqrt{E [\text{GeV}]} \oplus 100 \text{ ps}$ , respectively. For this analysis, the trigger [10] uses only calorimeter information. Two energy deposits above threshold ( $E > 50$  MeV for the barrel and  $E > 150$  MeV for endcaps) are required. Recognition and rejection of cosmic-ray events is also performed at the trigger level. Events with two energy deposits above a 30 MeV threshold in the outermost calorimeter plane are rejected.

The  $328 \text{ pb}^{-1}$  of data used in this analysis were collected in 2001 and 2002. The data are divided into 14 run periods of about  $25 \text{ pb}^{-1}$ /period. For each data period, we have a corresponding sample of Monte Carlo (MC) events with approximately equivalent statistics.

## 3 Monte Carlo generators

The KLOE MC generates only radiation from IB, so a dedicated generator for DE is needed. Moreover, the accuracy of the KLOE IB generator is a relevant issue. The KLOE generator [11] uses a resummation in the soft-photon limit to all orders in  $\alpha$  of the  $\mathcal{O}(p^2)$  amplitude for single photon emission. It describes the IB photon spectrum at the

level of  $\sim 1\%$ , which is appropriate for inclusive decay-rate measurements at the 0.1% level. However, since the DE contribution is about 1% of the IB contribution, the accuracy level of the KLOE IB generator is of about the same order as the DE contribution itself. From the point of view of the measurement of  $R$ , this could introduce an error of only  $\sim 1\%$ . On the other hand, a fit-based counting procedure making use of an IB distribution biased by  $\sim 1\%$  could introduce a  $\sim 100\%$  error in the number of  $K_{e3\gamma}^0$  events from DE. Therefore, in this analysis, we use the generator of [1] to describe the photon spectrum from IB as well as from DE. This generator is based on an  $\mathcal{O}(p^6)$  calculation; the code was provided by the authors. The generator is incorporated into the KLOE MC and reconstruction program. This is the first analysis of the double differential spectrum to make use of an  $\mathcal{O}(p^6)$  generator.

## 4 Analysis

The criteria used to select an inclusive sample of  $K_{e3}^0$  events are the same described in [12]. We briefly summarize them here.

Candidate  $K_L$  events are tagged by the presence of a  $K_S \rightarrow \pi^+\pi^-$  decay. The tagging efficiency is independent of  $E_\gamma^*$  and  $\theta_\gamma^*$ . Over the range of  $E_\gamma^*$  the efficiency fluctuates around 66% with an rms of 0.3%; over the range of  $\theta_\gamma^*$  the rms fluctuation is 0.1%.

We search for a  $K_L$  decay along the direction of the  $K_L$  momentum as reconstructed from the  $K_S \rightarrow \pi^+\pi^-$  decay (*tagging line*). All tracks in the chamber, after removal of those from the  $K_S$  decay and their descendants, are extrapolated to their points of closest approach (PCA) to the tagging line. For each track candidate, we evaluate the distance  $d_{\text{PCA}}$  of closest approach to the tagging line. The length of extrapolation of the track to this point of closest approach,  $l_{\text{PCA}}$ , is also computed. Tracks satisfying  $d_{\text{PCA}} < ar_{xy} + b$ , with  $a = 0.03$  and  $b = 3$  cm, and  $-20 \text{ cm} < l_{\text{PCA}} < 25 \text{ cm}$  are accepted as  $K_L$  decay products, where  $r_{xy}$  is the distance of the vertex from the origin in the transverse plane. For each sign of charge we consider the track with the smallest value of  $d_{\text{PCA}}$  to be associated to the  $K_L$  decay. Starting from these track candidates, a two-track vertex is reconstructed. An event is retained if the vertex is in the fiducial volume  $35 \text{ cm} < r_{xy} < 150 \text{ cm}$  and  $|z| < 120 \text{ cm}$ . The tracking and vertex efficiencies are evaluated by MC simulation and corrected using data control samples [12, 13].

To remove background from  $K_L \rightarrow \pi^+\pi^-\pi^0$  and  $K_L \rightarrow \pi^+\pi^-$  decays with minimal efficiency loss, we apply loose kinematic cuts. Assuming the two tracks to have the pion mass, we require  $E_{\text{miss}}^2 - p_{\text{miss}}^2 - M_{\pi^0}^2 < -5000 \text{ MeV}^2$  and  $\sqrt{E_{\text{miss}}^2 + p_{\text{miss}}^2} > 10 \text{ MeV}$ , where  $E_{\text{miss}}$  and  $\mathbf{p}_{\text{miss}}$  are the missing energy and momentum, respectively. A large amount of background from  $K_L \rightarrow \pi\mu\nu$  decays is rejected using the variable  $\Delta_{\pi\mu}$ , the lesser value of  $|E_{\text{miss}} - p_{\text{miss}}|$  calculated in the two hypotheses,  $\pi\mu$  or  $\mu\pi$ . We retain events only if this variable is greater than 10 MeV.

These kinematic criteria do not provide enough suppression of the background from  $K_L \rightarrow \pi e \nu$  decays with incorrect track-particle assignment and from  $K_L \rightarrow \pi\mu\nu$  decays. We make use of time-of-flight (TOF) information from the calorimeter to further reduce the contamination [12]. For each  $K_L$  decay track with an associated cluster, we define the variable:  $\Delta t_i = t_{\text{clu}} - t_i$ , ( $i = \pi, e$ ) in which  $t_{\text{clu}}$  is the cluster time and  $t_i$  is the expected time of flight, evaluated according to a well-defined mass hypothesis. An effective way to select the correct mass assignment,  $\pi e$  or  $e\pi$ , is obtained by choosing the lesser of  $|\Delta t_{\pi^+} - \Delta t_{e^-}|$  and  $|\Delta t_{\pi^-} - \Delta t_{e^+}|$ . After the mass assignment has been made, we consider the variables  $\Delta t_{\pi^+} + \Delta t_e$  and  $\Delta t_{\pi^-} - \Delta t_e$ . We select the signal by using a  $2\sigma$  cut, where the resolution  $\sigma \simeq 0.5 \text{ ns}$ . We take the TOF efficiency from the Monte Carlo after correcting the time response of the calorimeter using data control samples [14].

For the purposes of track-to-cluster association, we define two quantities related to the distance between the extrapolation of the track to the calorimeter entry point and the nearest cluster:  $d_{\text{TC}}$ , the distance from the extrapolated entry point to the cluster centroid, and  $d_{\text{TC}\perp}$ , the component of this distance in the plane transverse to the momentum of the track at the entry position. We only consider clusters with  $d_{\text{TC}\perp} < 30 \text{ cm}$ . We evaluate the clustering efficiency using the Monte Carlo, and correct it with the ratio of data and Monte Carlo efficiencies obtained from control samples [12].

The inclusive  $K_{e3}^0$  reconstruction efficiency is about 0.25 and differs by  $\sim 6\%$  for  $K_L \rightarrow \pi^+e^-\bar{\nu}$  and  $K_L \rightarrow \pi^-e^+\nu$  events (see [12]). We therefore count the number of  $K_{e3}^0$  events separately for each charge. In all, we find about 3.5 million  $K_{e3}^0$  events with a contamination of  $7 \times 10^{-3}$  mainly due to  $K_L \rightarrow \pi^+\pi^-\pi^0$  and  $K_L \rightarrow \pi\mu\nu$  decay events.

We select signal  $K_{e3\gamma}^0$  events from within the inclusive  $K_{e3}^0$  sample. We first search for events with a photon cluster, i.e., a calorimeter cluster not associated with any track. Assuming that the  $K_L$  decay vertex lies on the tagging line, the arrival time of each photon gives an independent determination of the  $K_L$  decay position,  $\mathbf{x}_N$ , the so-called neutral vertex. The method is fully described in [9, 15]. We require that the distance  $d_{\text{NC}}$  between the position  $\mathbf{x}_N$  of the neutral vertex and the position  $\mathbf{x}_C$  of the  $K_L$  vertex determined by track reconstruction, to be within eight times the rms of the  $d_{\text{NC}}$  distribution for MC signal events. If there is more than one photon candidate, we choose the one with the smallest value of  $d_{\text{NC}}$ . We retain events reconstructed with  $\theta_\gamma^* > 20^\circ$ .

To evaluate the photon energy we use the track momenta and the photon cluster position. Specifically, we write for the photon momentum

$$\mathbf{p}_\gamma = E_\gamma \frac{\mathbf{x}_{\text{clu}} - \mathbf{x}_N}{|\mathbf{x}_{\text{clu}} - \mathbf{x}_N|}, \quad (4)$$

and for the missing four-momentum

$$p_\nu = p_K - p_\pi - p_e - p_\gamma, \quad (5)$$

where  $p_\nu, p_K, p_\pi, p_e$ , and  $p_\gamma$  are the particle four-momenta. Setting  $p_\nu^2 = 0$  and solving the above equations gives  $E_\gamma$ ,

the photon energy in the laboratory system, with a resolution of  $\sim 1$  MeV. This resolution is about a factor of ten better than that obtained using the energy measurement from the calorimeter.

The main background contribution at this stage is from  $K_{e3\gamma}^0$  events with an undetected soft photon to which a cluster from machine background has been accidentally associated. This background is strongly reduced by requiring  $E_{\text{clu}} > 25$  MeV, where  $E_{\text{clu}}$  is the cluster energy as measured in the calorimeter, and by cutting on the difference between  $E_{\text{clu}}$  and  $E_\gamma$  as shown in Fig. 1. We reduce the relative contribution from background by a factor of four, with  $\sim 7\%$  loss in signal efficiency.

The background contributions from  $K_L \rightarrow \pi^+\pi^-\pi^0$  and  $K_L \rightarrow \pi\mu\nu$  events after application of the above cuts are 4.2% and 2.5%, respectively. The reconstructed photon energy and angular distributions for background events from these sources overlap with those for DE events. We use neural network techniques to reduce these backgrounds. To remove  $K_L \rightarrow \pi^+\pi^-\pi^0$  events, we use a neural network based on the photon energy and angle (with respect to the momentum of the lepton candidate), the track momenta, the missing momentum, and  $M_{\gamma\nu}^2$ , the invariant mass of the photon-neutrino pair. To remove  $K_L \rightarrow \pi\mu\nu$  events, we use a neural network based on the track momenta, the calorimeter energy measurement, and the cluster centroid position. Cuts on the neural network output reduce background from  $K_L \rightarrow \pi^+\pi^-\pi^0$  decays from 4.2% to 0.4%, and from  $K_L \rightarrow \pi\mu\nu$  decays, from 2.5% to 1.4%. The signal loss is 10%. Figure 2 shows the selection efficiency for signal events after all cuts, relative to the inclusive  $K_{e3}^0$  sample, as evaluated by MC. Averaged over the spectrum of  $E_\gamma^*$ , the absolute efficiency

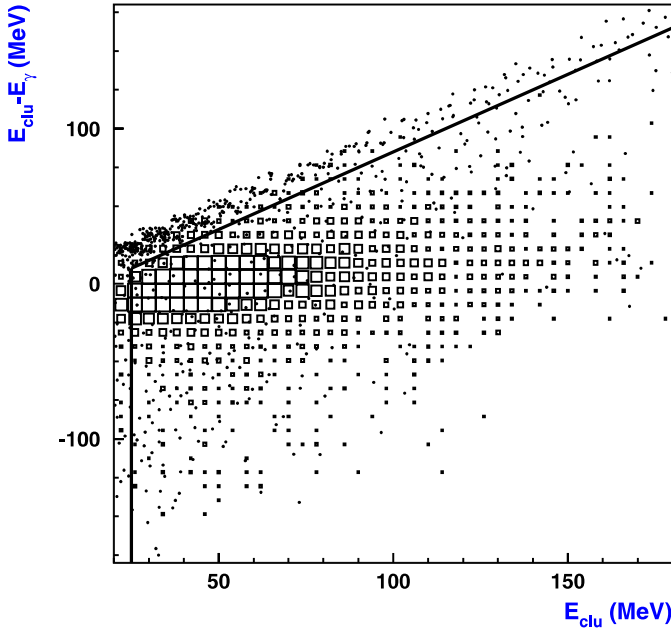


**Fig. 1.** Cut used to remove events with accidental activity (dots) from the sample of signal  $K_{e3\gamma}^0$  events (boxes), in MC simulation

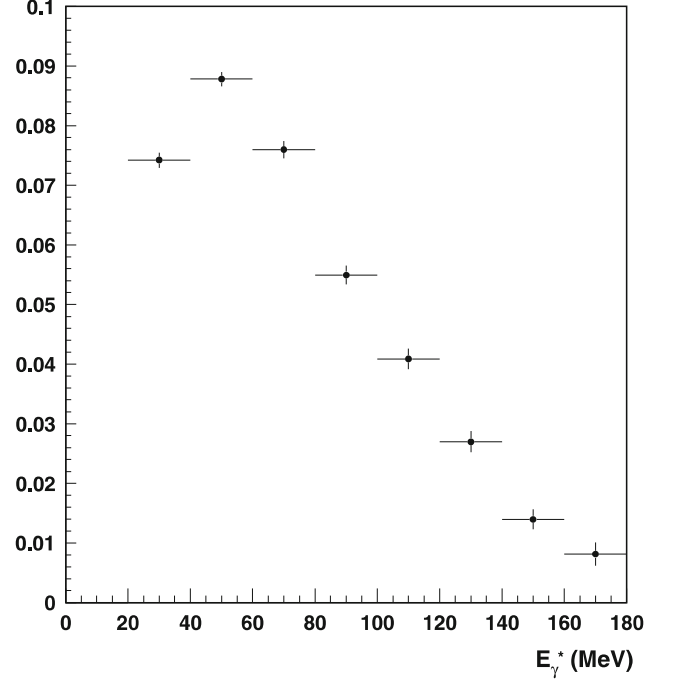


**Fig. 2.**  $K_{e3\gamma}^0$  signal efficiency, relative to the sample of tagged  $K_L$  decays, from MC

for detection of a  $K_{e3\gamma}^0$  event from IB is  $(6.92 \pm 0.04)\%$ . Because the  $E_\gamma^*$  spectrum for DE events is harder, the average absolute detection efficiency in this case is slightly lower:  $(5.80 \pm 0.05)\%$ .

To check the data-MC agreement, calibrate the MC position  $\mathbf{x}_N$ , and correct the photon-selection efficiency, we use  $K_L \rightarrow \pi^+\pi^-\pi^0$  decays as a control sample. These events are selected using a tight cut in the variable  $E_{\text{miss}}^2 - p_{\text{miss}}^2 - m_{\pi^0}^2$ , evaluated assigning the pion mass to both tracks. We additionally require the presence of a cluster with  $E_{\text{clu}} > 60$  MeV not associated to any track, corresponding to one of the two photons from  $\pi^0$  decay. This high-energy photon is used to tag the presence of the second photon. We select about 350 000  $K_L \rightarrow \pi^+\pi^-\pi^0$  events with a purity of 99.8%.

We first compare the resolution for photon energy reconstruction in data and MC. We reconstruct the energy of the second photon using (4) and (5), where the tagging photon is ignored and plays the role of the undetected neutrino in signal events. The expected value of the energy of the second photon is computed using the reconstructed momentum of the tagging photon to close the kinematics at the decay vertex. Figure 3 shows the distribution of the residuals for both data and MC. Good agreement is observed.

In addition, we use the  $K_L \rightarrow \pi^+\pi^-\pi^0$  control sample to check the reconstruction of the distance  $d_{NC}$  and its rms in both data and MC in order to tune the MC simulation (see Fig. 4).

We also use the  $K_L \rightarrow \pi^+\pi^-\pi^0$  sample to validate the MC simulation of the calorimeter energy response, since we apply analysis cuts on  $E_{\text{clu}}$  to remove accidentals. The en-

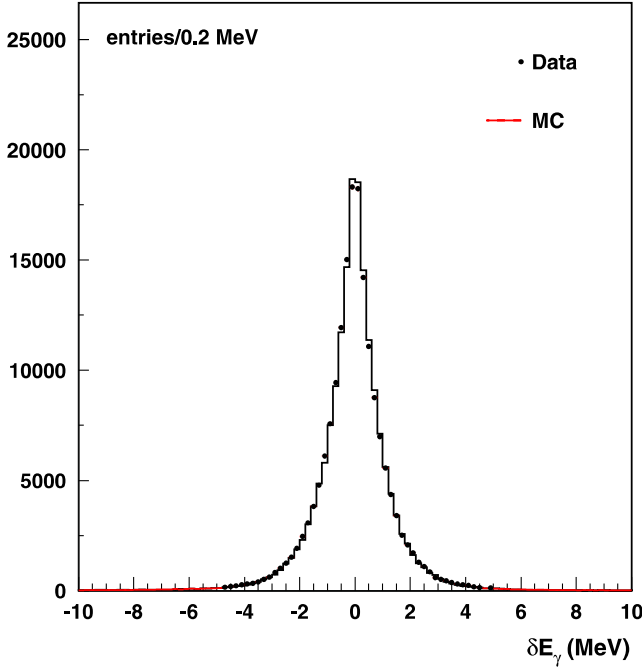


**Fig. 3.** Comparison of resolution for photon energy reconstruction for  $K_L \rightarrow \pi^+ \pi^- \pi^0$  events in data and MC

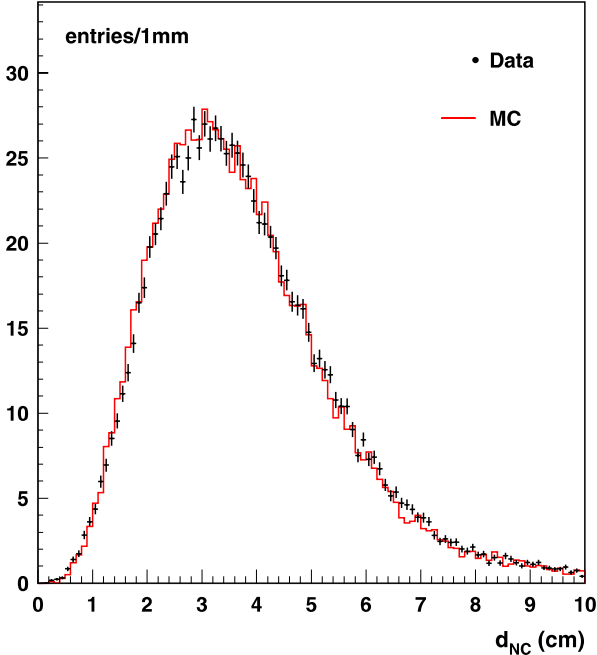


**Fig. 4.** Comparison of  $d_{NC}$  distributions for data and MC for  $K_L \rightarrow \pi^+ \pi^- \pi^0$  vertices in the central part of the drift chamber, after corrections

ergy scale is about 2 MeV lower in MC than in data. To good approximation, this bias is independent of energy.

Finally, we use the  $K_L \rightarrow \pi^+ \pi^- \pi^0$  sample to evaluate the photon selection efficiency for data and MC. We obtain a correction of a few percent, which we apply to the simulation. Further details can be found in [16].

## 5 Fit

We perform a fit to the experimental distribution in  $(E_\gamma^*, \theta_\gamma^*)$  using the sum of four independently normalized MC distributions:

- The distribution for  $K_{e3\gamma}^0$  events from IB satisfying the kinematic cuts  $E_\gamma^* > 30$  MeV and  $\theta_\gamma^* > 20^\circ$  as generated;
- The distribution corresponding to the function  $f(E_\gamma^*)$  in the second term of (1), representing the modification of the spectrum from DE events satisfying the kinematic cuts as generated;
- $K_{e3\gamma}^0$  events from IB *not* satisfying the kinematic cuts as generated;
- Physical background from  $K_L \rightarrow \pi^+ \pi^- \pi^0$  and  $K_L \rightarrow \pi \mu \nu$  events.

These four MC distributions are shown in Fig. 5. The free parameters of the fit are the number of IB events, the effective number of DE events (the integral of the spectral distortion induced by the IB–DE interference), and the number of  $K_{e3\gamma}^0$  events not satisfying the kinematic cuts. We fix the background contribution from  $K_L \rightarrow \pi^+ \pi^- \pi^0$  and  $K_L \rightarrow \pi \mu \nu$  using the MC. Figure 6 shows the result of the fit. The two-dimensional distributions are plotted on a single axis; the  $E_\gamma^*$  distributions for each of the eight slices in  $\theta_\gamma^*$  are arrayed sequentially. The eight slices in  $\theta_\gamma^*$  are  $20^\circ$  each and cover the interval from  $20^\circ$  to  $180^\circ$ . The values obtained for the fit parameters are listed, together with their correlation coefficients, in Table 1. The fit gives  $\chi^2/\text{ndf} = 60/69$  ( $P = 77\%$ ). The negative value for the effective number of counts from DE events is a result

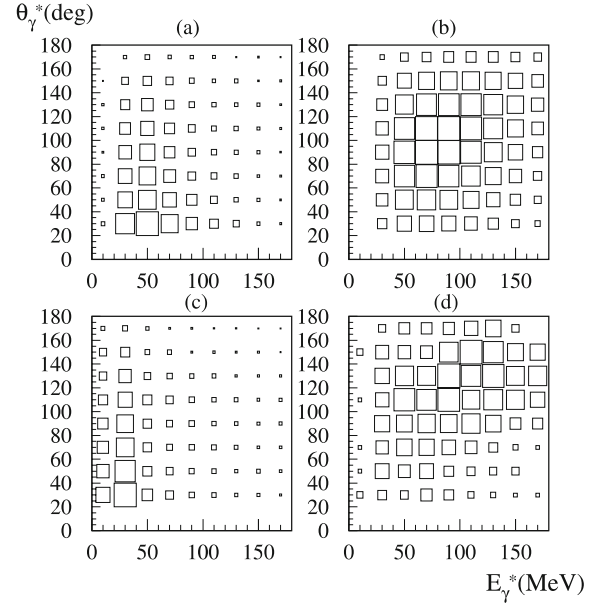


**Fig. 5.** Reconstructed Monte Carlo distributions in  $\theta_\gamma^*$  (deg) vs.  $E_\gamma^*$  (MeV). From top left: **a**  $K_{e3\gamma}^0$  events from IB, **b**  $K_{e3\gamma}^0$  events from DE as defined in the text, **c**  $K_{e3\gamma}^0$  events from IB not satisfying the  $E_\gamma^*$  and/or  $\theta_\gamma^*$  cuts as generated, **d** background events from  $K_L \rightarrow \pi^+ \pi^- \pi^0$  and  $K_L \rightarrow \pi \mu \nu$ . The statistics for different plots do not respect natural proportions

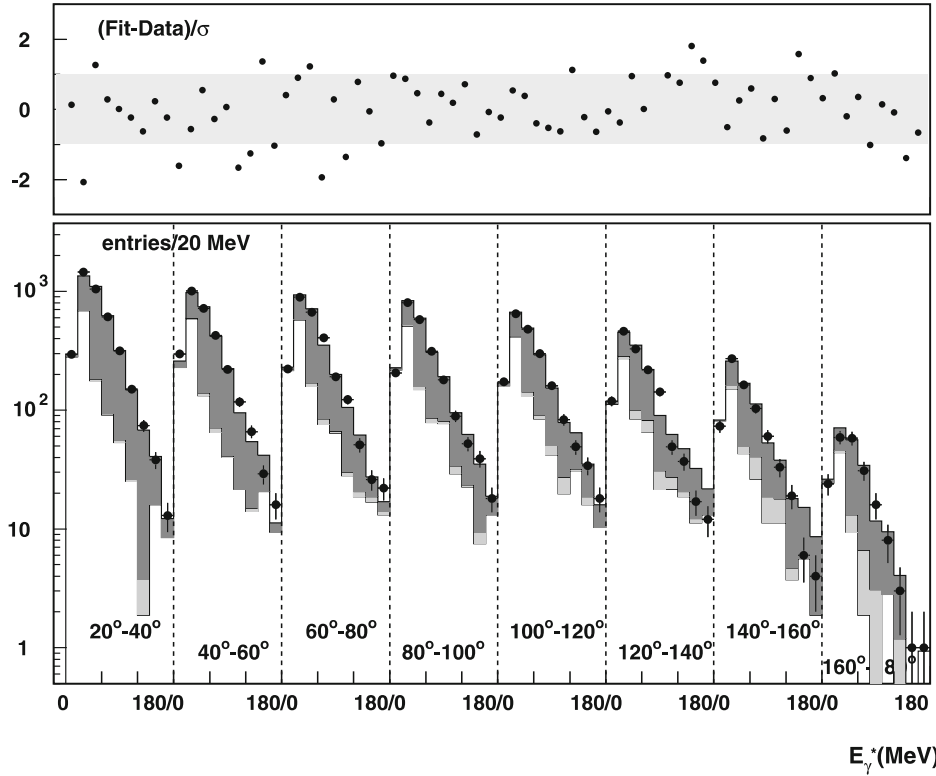


**Fig. 6.** Results of fit to  $(E_\gamma^*, \theta_\gamma^*)$  distribution: *dots* show data, *dark gray region* shows contribution from  $K_{e3\gamma}^0$  events (IB and DE) satisfying kinematic cuts, *white region* shows contribution from  $K_{e3\gamma}^0$  events not satisfying cuts, *light gray region* shows contribution from  $K_L \rightarrow \pi^+\pi^-\pi^0$  and  $K_L \rightarrow \pi\mu\nu$  decays. *Above*: normalized fit residuals

**Table 1.** Values obtained for fit parameters, with correlations

Contribution	$N$	$\delta N$	Correlation coeffs.		
IB	9083	213	1		
$K_{e3\gamma}^0$ not in cuts	6726	194	-0.586		
DE (effective)	-102	59	-0.254	-0.022	1

of the destructive interference between the IB and DE amplitudes. The presence of DE modifies the total number of  $K_{e3\gamma}^0$  events satisfying the kinematic cuts at the level of  $\sim 1\%$ . From the fit results, we obtain

$$R \equiv \frac{\Gamma(K_{e3\gamma}^0; E_\gamma^* > 30 \text{ MeV}, \theta_\gamma^* > 20^\circ)}{\Gamma(K_{e3}^0)} = (924 \pm 23_{\text{stat}}) \times 10^{-5}.$$

## 6 Systematic uncertainties

We estimate systematic uncertainties by varying the selection cuts. Signal events are defined by the tracking, clustering, track-to-cluster association, neutral-vertex acceptance, and analysis cuts. Any variation of these cuts produces a variation in the result.

**Tagging.** In obtaining our result, we do not require that the tagging  $K_S \rightarrow \pi^+\pi^-$  decay by itself satisfy the calorimeter trigger. This requirement may be imposed by

demanding the identification of two clusters that are associated to tracks from the  $K_S \rightarrow \pi^+\pi^-$  decay and which fire trigger sectors. Doing this makes the analysis independent of the MC estimate of the trigger efficiency, at a cost in statistics. When we impose this requirement as a check, we observe a variation  $\Delta R = 4 \times 10^{-5}$ .

**Tracking.** The most selective variable in the definition of track candidates is  $d_{\text{PCA}}$ , the distance of closest approach of the track to the tagging line. As described in Sect. 4, we accept tracks with  $d_{\text{PCA}} < a r_{xy} + b$ , with  $a = 0.03$  and  $b = 3$  cm.  $d_{\text{PCA}}$  is reconstructed with a resolution of about 1 cm. The tracking efficiency depends most sensitively on the value of  $b$ . We vary  $b$  from 2 to 5 cm and re-evaluate the run-period-dependent tracking efficiency correction in each case. The uncertainty on the tracking efficiency correction is dominated by sample statistics. We observe a variation in the result  $\Delta R = 1.5 \times 10^{-5}$ . The width of the  $l_{\text{PCA}}$  distribution is  $\sim 4$  cm, so that the cut on  $l_{\text{PCA}}$  is quite loose ( $\sim 5\sigma$ ), and we assign no corresponding contribution to the systematic error.

**Clustering.** The most selective variable used for track-to-cluster association is the transverse distance  $d_{\text{TC}\perp}$ . This distance is reconstructed with a resolution of about 6 cm. We vary the cut on  $d_{\text{TC}\perp}$  from 15 to 50 cm, around a nominal value of 30 cm. For each value of  $d_{\text{TC}\perp}$ , we re-evaluate the clustering efficiency correction, which is run-period dependent. Here also, the uncertainty in the correction is dominated by sample statistics. We observe a variation  $\Delta R = 5.5 \times 10^{-5}$ .

**Kinematic cuts.** We apply loose kinematic cuts. When these cuts are varied, the variation in the result is negligible.



**TOF cuts.** TOF cuts are used in the identification of the inclusive  $K_{e3}^0$  sample. When the TOF cut is varied by 30% around its nominal  $2\sigma$  value, we observe a variation in the result  $\Delta R = 1.3 \times 10^{-5}$ .

**Momentum miscalibration and resolution.** We have also considered effects from the momentum scale accuracy and resolution. We assume a maximum momentum scale uncertainty of 0.1% [15], which corresponds to a variation in the result  $\Delta R = 3.5 \times 10^{-5}$ . Changing the value assumed for the momentum resolution by  $\pm 3\%$  as in [12] gives rise to a variation  $\Delta R = 7.2 \times 10^{-5}$ .

**Fiducial volume.** Reducing the fiducial volume by 20% produces a variation in the result  $\Delta R = 3 \times 10^{-5}$ .

**Rejection of accidentals.** The cut used to remove accidentally associated background clusters is illustrated in Fig. 1. The cut is tightest at lower energies. At  $E_{\text{clu}} = 25$  MeV, we require  $E_{\text{clu}} - E_\gamma < 10$  MeV, while for signal events the variance of this residual is  $\sim 8$  MeV. Varying the intercept of this cut by  $\pm 5$  MeV gives rise to a variation in the result  $\Delta R = 5.2 \times 10^{-5}$ .

**Neutral-vertex acceptance.** We search for a neutral vertex within a sphere centered around  $\mathbf{x}_C$ . We accept events for which  $d_{\text{NC}}$  is less than eight times the rms of the  $d_{\text{NC}}$  distribution for signal events. We vary the cut from six to ten times the rms of the distribution and observe a variation in the result  $\Delta R = 2.9 \times 10^{-5}$ .

**Background.** Conservatively, we remove the cuts on the neural network outputs. This increases the background level by nearly a factor of four. The variation in the result is  $\Delta R = 9 \times 10^{-5}$ .

**Fit systematics.** As a check, we perform the fit leaving free the number of background events from  $K_L \rightarrow \pi^+ \pi^- \pi^0$  and  $K_L \rightarrow \pi \mu \nu$ . This gives consistent results, but with a greater statistical uncertainty. In particular, the total number of background events from the fit is  $406 \pm 152$ , as compared to the MC expectation,  $301 \pm 17$ . We have also checked the fit stability as a function of run period. This requires fixing the number of background events, because within a single run period, the background statistics are too low to guarantee good fit convergence. In addition, we do not include DE, as the data from a single run period offer no sensitivity to this

component. The stability over run periods is good: a fit to determine the average value of  $R$  gives  $\chi^2/\text{ndf} = 9/13$ . Therefore, we assign no contribution to the systematic uncertainty from this source.

All systematic errors are summarized in Table 2. These errors are added in quadrature to obtain the final systematic error.

## 7 Results

Our final result for  $R$  is

$$R = (924 \pm 23_{\text{stat}} \pm 16_{\text{syst}}) \times 10^{-5}.$$

The value of the parameter  $\langle X \rangle$  defined in (1) is derived from the result of the fit that gives the effective numbers of IB and DE events, taking into account the difference in the overall detection efficiencies for each type (the detection efficiency for IB events is  $\sim 20\%$  higher than for DE events). We obtain

$$\langle X \rangle = -2.3 \pm 1.3_{\text{stat}} \pm 1.4_{\text{syst}}.$$

The systematics on  $\langle X \rangle$  are evaluated in the same manner as for  $R$ , and the different contributions are listed in Table 2. The correlation coefficient between the total errors on  $R$  and  $\langle X \rangle$  is 3.9%. The  $1\sigma$  contour is illustrated in Fig. 7.

The dependence of  $R$  on  $\langle X \rangle$  of (3) is shown in Fig. 7 as the diagonal shaded band. This dependence can be used to further constrain the possible values of  $R$  and  $\langle X \rangle$  from

**Table 2.** Summary of the absolute systematic uncertainties on  $R$  and  $\langle X \rangle$

Source	$10^5 \times \Delta R$	$\Delta \langle X \rangle$
Tagging	4.0	0.7
Tracking	1.5	0.8
Clustering	5.5	0.1
TOF cut	1.3	0.5
$p$ miscalibration	3.5	0.2
$p$ resolution	7.2	0.4
Fiducial volume	3.0	0.5
Accidentals	5.2	0.4
Neutral vertex acceptance	2.9	0.3
Background	9.0	0.1
Total	15.5	1.4

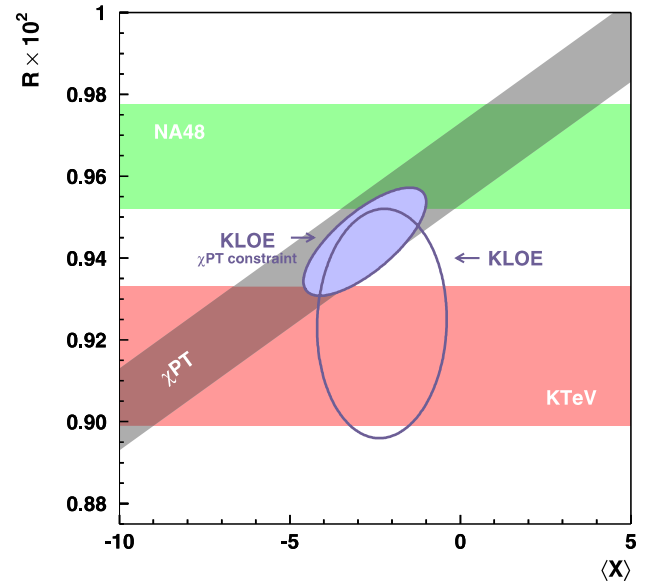


**Fig. 7.** KLOE  $1\sigma$  contours in the  $(R, \langle X \rangle)$  plane from fit to the  $(E_\gamma^*, \theta_\gamma^*)$  distribution (*open ellipse*), and same results when combined with constraint from  $\chi\text{PT}$  (*filled ellipse*). Results from KTeV and NA48 are also shown, as well as the dependence of  $R$  on  $\langle X \rangle$  according to (3), used as the constraint

our measurement, giving the  $1\sigma$  contour illustrated as the filled ellipse in the figure. The constraint is applied via a fit, which gives  $R = (944 \pm 14) \times 10^{-5}$  and  $\langle X \rangle = -2.8 \pm 1.8$ , with correlation  $\rho = 72\%$  and  $\chi^2/\text{ndf} = 0.64/1$  ( $P = 42\%$ ). This result represents an improved test of  $\chi$ PT with respect to that obtained using the measurements of  $R$  from [6, 7].

Finally, to test the accuracy of the  $\mathcal{O}(p^2)$  KLOE IB generator [11], we have performed fits to the data with no DE component. We obtain

$$\begin{aligned} \mathcal{O}(p^6) \text{ generator [1]} & \quad R = (925 \pm 23_{\text{stat}}) \times 10^{-5}; \\ \mathcal{O}(p^2) \text{ generator [11]} & \quad R = (921 \pm 23_{\text{stat}}) \times 10^{-5}. \end{aligned}$$

The fit with the  $\mathcal{O}(p^6)$  generator gives  $\chi^2/\text{ndf} = 63/70$  ( $P = 71\%$ ); that with the  $\mathcal{O}(p^2)$  generator gives  $\chi^2/\text{ndf} = 68/70$  ( $P = 55\%$ ). The agreement between these results confirms the reliability of the KLOE generator for IB events.

## 8 Conclusion

Two different components contribute to photon emission in  $K_{e3\gamma}^0$  decays: IB and DE. The latter describes photon radiation from intermediate hadronic states, providing additional information on the hadronic structure of the kaon.  $\chi$ PT predicts that the IB and DE amplitudes interfere, resulting in a negative effective strength  $\langle X \rangle$ . From a fit to the  $(E_\gamma^*, \theta_\gamma^*)$  distribution for  $K_{e3\gamma}^0$  decays based on  $\mathcal{O}(p^6)$   $\chi$ PT calculations, we obtain a value for  $R$  and a first measurement of  $\langle X \rangle$ . These results, which favor destructive interference between the IB and DE amplitudes, are good agreement with the  $\chi$ PT predictions.

*Acknowledgements.* We would like to thank Bastian Kubis, one of the authors of [1], for providing the Monte Carlo generator used in this analysis. We thank the DAΦNE team for their efforts in maintaining low-background running conditions and their collaboration during all data taking. We want to thank our technical staff: G.F. Fortugno and F. Sborzacchi for their dedicated work to ensure efficient operation of the KLOE Computing Center; M. Anelli for his continuous support to the gas system and the safety of the detector; A. Balla, M. Gatta,

G. Corradi and G. Papalino for maintenance of the electronics; M. Santoni, G. Paoluzzi and R. Rosellini for general support to the detector; C. Piscitelli for his help during major maintenance periods. This work was supported in part by EURODAPHNE, contract FMRX-CT98-0169; by the German Federal Ministry of Education and Research (BMBF), contract 06-KA-957; by the German Research Foundation (DFG), ‘Emmy Noether Programme’ contracts DE839/1-4; by INTAS, contracts 96-624 and 99-37; and by the EU Integrated Infrastructure Initiative HadronPhysics Project, contract RII3-CT-2004-506078.

## References

1. J. Gasser, B. Kubis, N. Paver, M. Verbeni, Eur. Phys. J. C **40**, 205 (2005)
2. B. Kubis, private communication
3. KTeV Collaboration, A. Alavi-Harati et al., Phys. Rev. D **64**, 112004 (2001)
4. H.W. Fearing, E. Fischbach, J. Smith, Phys. Rev. D **2**, 542 (1970)
5. M.G. Doncel, Phys. Lett. B **32**, 623 (1970)
6. KTeV Collaboration, T. Alexopoulos et al., Phys. Rev. D **71**, 012001 (2005)
7. NA48 Collaboration, A. Lai et al., Phys. Lett. B **605**, 247 (2005)
8. M. Adinolfi et al., Nucl. Instrum. Methods A **488**, 51 (2002)
9. M. Adinolfi et al., Nucl. Instrum. Methods A **482**, 364 (2002)
10. M. Adinolfi et al., Nucl. Instrum. Methods A **492**, 134 (2002)
11. C. Gatti, Eur. Phys. J. C **45**, 417 (2006)
12. KLOE Collaboration, F. Ambrosino et al., Phys. Lett. B **636**, 166 (2006)
13. KLOE Collaboration, F. Ambrosino et al., Phys. Lett. B **632**, 43 (2006)
14. KLOE Collaboration, F. Ambrosino, et al., Phys. Lett. B **636**, 173 (2006)
15. KLOE Collaboration, F. Ambrosino et al., Nucl. Instrum. Methods A **534**, 403 (2004)
16. M. Antonelli, M. Dreucci, C. Gatti, Measurements of the radiative  $K_{e3}^0$  branching ratio and direct emission contribution in semileptonic decay  $K_{e3}^0$ , KLOE Note 216 (2007), <http://www.lnf.infn.it/kloe/pub/knote/kn216.ps>